RSC Advances

ROYAL SOCIETY OF CHEMISTRY

www.rsc.org/advances

Molecular dynamics study of Congo red interaction with carbon nanotubes

Tomasz Panczyk,[1,*] Pawel Wolski,[1] Anna Jagusiak, [2] Mateusz Drach,[3]

[1]*Institute of Catalysis and Surface Chemistry, Polish Academy of Sciences*
ul. Niezapominajek 8, 30239 Cracow, Poland
e-mail: panczyk@vega.umcs.lublin.pl

[2]*Chair of Medical Biochemistry, Jagiellonian University Medical College,*
ul. Kopernika 7, 31034 Cracow, Poland

[3]*Department of Chemistry, Maria Curie-Sklodowska University*
pl. M. Curie-Sklodowskiej 3, 20031 Lublin, Poland

Abstract

This work deals with molecular dynamics simulations of Congo red (CR) interaction with carbon nanotubes (CNT). We studied several combinations of systems parameters in order to assess how the nanotube diameter and Congo red density affect the structure and stability of CNT-CR conjugates at various pH conditions. We found that, at the considered conditions, the CR binds strongly to the CNT surfaces and the CNT-CR conjugates are thermodynamically stable according to the determined values of free energies. Adsorption on wider nanotubes is stronger than on the narrow ones and larger densities of CR on the CNT surfaces lead to weakening of biding energy per single CR molecule. Changes of pH, that is varying concentration of protonated and deprotonated forms of CR, lead to significant changes in binding energies as well as to qualitative changes of the structure of the adsorbed CR. It was found that at pH > 5.5 the CR molecules readily occupy inner cavities of the nanotubes. Upon lowering pH the occupation of the inner space of CNTs is strongly reduced and the preferred configuration is formation of a densely packed CR layer on the sidewalls of the CNT. This effect can potentially be utilized in pH controlled corking/uncorking of carbon nanotubes in water solutions.

1. Introduction

Pristine carbon nanotubes (CNT) exist normally in the form of ropes consisting of individual graphene cylinders and are insoluble in water. In many areas of applications solubility of CNTs in aqueous media is, however, a crucial condition. Therefore, many methods of fabrication of water soluble CNTs were proposed in the literature. They can be divided into two general approaches; (i) covalent functionalization of sidewalls, defect sites or tips[1,2] and (ii) noncovalent attachment of various molecules providing hydrophilic functional groups.[3,4,5] The noncovalent attachment leads to chemical and topological structure of the nanotubes intact[3], thus, in many cases, this is the preferred approach.

Among many possible choices of agents leading to water soluble or even biocompatible CNTs[6,7] the Congo Red (CR) reveals very promising properties. As found experimentally, the mixture of CNTs and CR can be dissolved in water with the solubility as high as 3.5 mg mL^{-1} for CNTs.[4] Congo Red, compound from the group of bisazo dyes, associates in aqueous solutions forming supramolecular assemblies of a polyanionic nature. That structure can bind to the surface of homopolymers (like cellulose) and proteins forming the ordered amyloid-like organization of protein aggregates.[8]Another important feature of CR is the ability to selectively interact with antigen-complexed antibodies, which opens possibilities for use of CR in the targeted transport of drugs.[9] Carbon nanotubes are known as promising nanotransporters for drugs and variety of factors are being studied to make them biocompatible and controllable in biological environment.[10,11,12] Thus, the CNT-CR conjugates are definitely worth of closer analysis mainly in terms of their microscopic structure and its changes with pH, density or CNT parameters.

The aim of our studies is therefore the microscopic analysis of the interaction of CR molecules with carbon nanotubes in water (or physiological fluid). Those studies are based on molecular dynamics methodology, thus, we can directly analyze the topology and thermodynamics of the systems. Among useful conclusions concerning the structure and stability of the CNT-CR conjugates we also found one very interesting feature. Namely, depending on pH the CR molecules readily locate in the CNT interior or prefer adsorption on the sidewalls. This effect can be utilized in pH controlled corking/uncorking of carbon nanotubes.

2. Methods

Molecular dynamics simulations of CR in aqueous solution have been reported in the literature.[13] Generally, two approaches were used for construction of the force field: charmm[14] and amber force fields.[15] Physically, there is no a big difference between the assumed force field parameters provided that the simulation protocol is compatible with the assumptions of a given

force field and functional forms of potential functions. Therefore, we utilized the generalized AMBER force field (GAFF)[16] in order to be compatible with other components of the studied system. The force field parameters and molecular topology of CR were obtained using antechamber program.[17] Partial charges (RESP, restrained electrostatic potential[18]) were taken from ref.[19] and summation of the electrostatic interactions was carried out using the Ewald summation methodology. Water molecules were accounted for explicitly using the TIP3P water model[20] as it is fully compatible with the AMBER force field. The force field associated with the CNT was based on the application of the aiREBO potential,[21] and the interactions of CR with CNT were described using non-bonded part of the AMBER force field. The calculations were performed using the open source lammps code[22] and generation of input files for lammps was done using self-designed scripts. We used 20 or 40 CR molecules in the simulation box depending on the size of the CNT being studied. At the beginning, the CR molecules were uniformly distributed within the simulation box but no molecules were placed inside the nanotube. Water molecules were kept rigid using the SHAKE algorithm. Na+ and Cl^- ions were added to the simulation box in the amounts accounting for the assumed ionic strength and pH values. The cutoff distance for both van der Waals and electrostatic interactions was 12 Å.

The calculations were carried out with the timestep 1.5 fs. The systems were kept at constant 310 K temperature and constant pressure 1 bar. Equilibrations of the systems were carried out at temperature 400 K and for 1.5 ns, afterwards the temperatures were reduced to 310K within 0.3 ns and next equilibrations were continued for 1.2 ns.

3. Results and Discussion

3.1 Molecular topology of CR at various pH

Congo red is a bisazo dye which at low pH changes color due to protonation of its amino groups and shift of electrons in the aromatic ring and azo-bond. The protonation of Congo red amino groups takes place at pH 4.5 – 5.5.[8] Thus, above pH 5.5 the dominant form of CR in solution is the deprotonated form shown in Fig.1. At low pH, it is believed, that protonation occurs at amino or azo nitrogens[23] leading to the protonated form shown in Fig.1 for the former case. Protonation of azo nitrogens leads to two tautomeric azonium and ammonium forms, as discussed in the literature.[23] These tautomeric forms cannot be adequately modeled using classical nonreactive force fields, thus we will focus on amino protonated form while studying conditions of low pH. Because protonation compensate the total charge of CR molecule it is believed that the choice of a particular protonated form of CR is not critical in terms of intermolecular interactions. This is because the electrostatic interactions usually dominate over other types of interactions and, in fact, determine

the overall behavior of the system under investigation.

Thus, in further considerations we will assume that at pH ≥ 5 all CR molecules are in the deprotonated form, whereas at pH ≤ 4 the protonated form for all CR molecules is assumed. We will also consider an intermediate case, that is half of the CR molecules is in the deprotonated form and the second half in the protonated one. Thus, this intermediate case should be representative of pH close to pKa, i.e. between 4.5 and 5.5. Obviously, in any case adequate amounts of Na^+ and Cl^- ions are incorporated to the simulation box to keep the ionic strength at the assumed level and preserve neutral charge of the system.

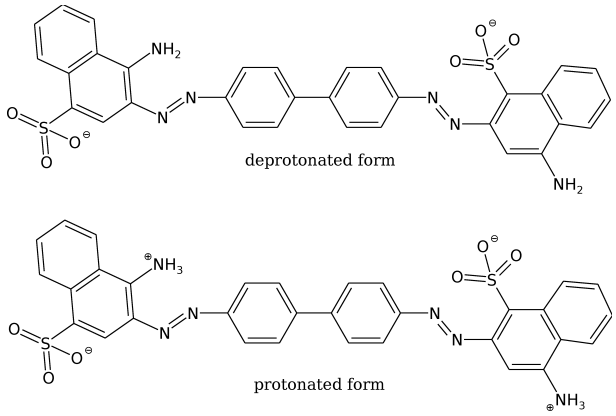

Figure 1. Structures of the studied deprotonated and protonated forms of Congo Red.

3.2 Structure of CR micelles at various pH

It is well known in literature that CR forms a rod-like or ribbon-like supramolecular mesophase in water solutions[24] due to mechanism of face-to-face stacking.[25] That mechanism is physically equivalent to enhanced dispersion interaction between aromatic rings due to relatively high atomic densities within the rings. The attractive dispersion interactions between CR molecules are compensated to some extent by repulsive electrostatic interaction. The range of that compensation will be, in turn, dependent on pH. Thus, in order to gain a deeper physical insight into the conditions leading to self-assembly of CR in solution we performed a series of simulations at various pH values for clusters of 20 CR molecules in solution.

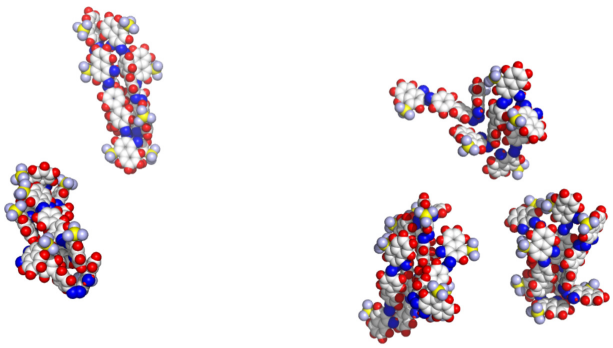

pH5: <U_{cc}>= 277 kJ/mol, 3 clusters
<U_T> =-553 kJ/mol

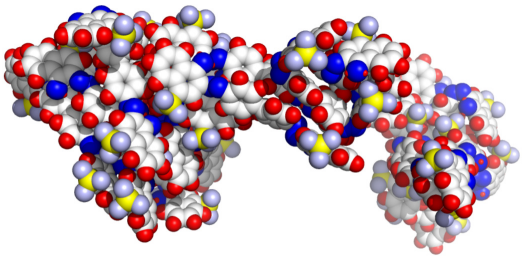

pH4: <U_{cc}>=-143 kJ/mol, 1 cluster
<U_T> =-897 kJ/mol

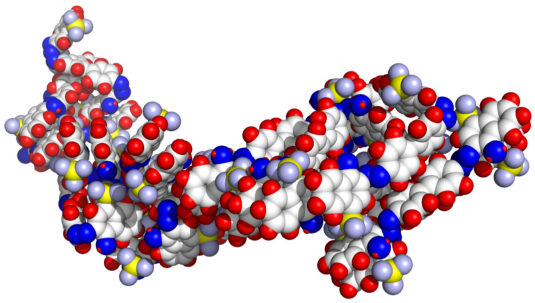

pH3: <U_{cc}>= -805 kJ/mol, 1 cluster
<U_T> =-1234 kJ/mol

Figure 2. Resulting structures of CR clusters obtained in simulations for 3 cases of pH. pH5 means that all 20 CR molecules are in the deprotonated form (Fig.1), for pH4 it is assumed that 10 molecules are in the deprotonated form and 10 in the protonated one, finally pH3 means that all 20 molecules are in the protonated form. The simulations were carried out for temperature 310 K and ionic strength 0.145 mol L^{-1}.

Fig.2 shows the resulting structures of CR clusters for the discussed 3 values of pH. We formally call these cases as pH3, pH4, and pH5 and they correspond to 20 protonated, 10 protonated and 10 deprotonated and 20 deprotonated forms of CR molecule, respectively. As we can see in the case pH5 the CR molecules form a few fully separated clusters in solution. Precisely, we found 2 clusters composed of 8 CR molecules and one 4-molecules cluster (the snapshot in Fig.2

suggests existence of 4 clusters but this is only a visual effect of periodic boundary conditions). For pH4 and pH3 we observed single 20-molecules clusters which seem to organize into ribbon-like micelles.

The energetic parameters, that is, mean interaction energy between CR molecules $<U_{cc}>$ and mean total interaction energy of CR molecule with its surrounding $<U_T>$ give us a notion about the role of protonation in self-assembly of CR into clusters. In the case pH5 the interaction between CR molecules is repulsive (positive energy) and this is due to electrostatic interactions between deprotonated molecules. However, the total potential energy of a given CR molecule is negative, thus the electrostatic repulsion is compensated by interaction with solvent molecules and the work related to breaking of solvent-solvent interaction network. Upon reducing pH the electrostatic repulsion is neutralized by the increasing amount of uncharged CR molecules. As we can see it is enough to make every second CR molecule uncharged (protonated) to get inversion of CR-CR interactions from repulsive to attractive (negative $<U_{cc}>$). In such cases the dispersion interactions (face-to-face stacking) probably dominate over the residual electrostatic repulsion which exists in case pH4. As a result we observe self-assembly of all CR molecules into a single cluster. The electrostatic repulsion is, of course, totally eliminated in the case pH3, thus both energies reach high negative values and, macroscopically, we should observe sedimentation of CR due to huge sizes of CR agglomerates.

The structure of CR clusters, as observed in simulation snapshots, seems to be consistent with the well-known empirical result, that is, CR molecules create ribbon-like micelles. However, in order to get a deeper quantitative description of those structures we defined two following parameters. The first parameter describes quantitatively the planarity of a single CR molecule. It was defined as the coefficient of determination R^2 found in fitting a plane to the position of all aromatic carbons in every single CR molecule. The fittings were done using 3D linear regression method and coefficients of determination R^2 were calculated according to the definition. Having determined the parameters of best-fitting planes we were also able to determine the components of vectors normal to the planes. In that way we could calculate the distribution of angles α between any two CR molecules as the angles between the best-fitting planes.

Fig. 3 shows histograms of R^2 and cos α determined within 1.2 ns runs for the analyzed systems. These histograms inform about the occurrence (probability of observation) of a given value in the considered system. We can, thus, conclude that majority of CR molecules keep planar configuration in all analyzed systems because maximum of the occurrence is located for $R^2>0.9$. However, none of the molecules is perfectly flat. There is also a significant fraction of molecules with small values of R^2 meaning that the preferred planar configuration is sometimes not reached.

The highest degrees of planarity reveal molecules for the pH5 case. This is due to formation of small clusters composed of a few molecules. Within such small clusters the molecules can easily reach the face-to-face configuration and stay in it for longer times. In the case of big clusters, i.e. in cases pH4 and pH3, the planarity is weaker, this is obviously due to more complex topology of the clusters and strong intermolecular interactions.

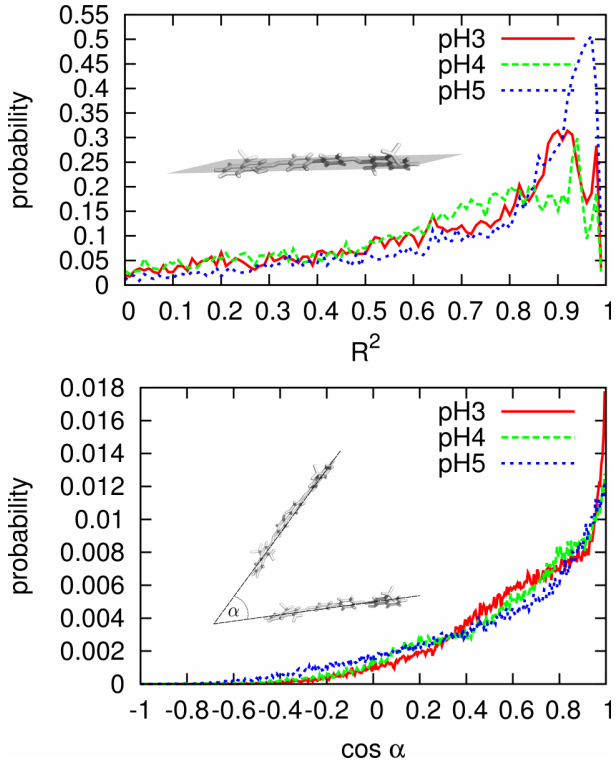

Figure 3. Histograms of the planarity parameter R^2 defined as the coefficient of determination in 3D linear regression of a plane to the positions of all aromatic carbons in the CR molecule, and, histogram of the angles between any two CR molecules in the system.

The distribution of the angles between CR molecules in Fig.3 implies that in any analyzed case the molecules form ribbon-like structures. The most dominant angle is 0 deg, that is, parallel orientation is the most probable. The fraction of perpendicular molecules is nonzero but it is small when compared to the fraction of almost or fully parallel molecules. It seems that in the case pH3 the CR aggregates are the most ordered because the maximum at cos α = 1 is the highest.

3.3 Interaction of CR with carbon nanotubes

Aromatic compounds are known to interact strongly with graphitic sidewalls of CNTs through effective π-π stacking.[26] These interactions manifest in solubilization of CNTs in aromatic solvents as well as solubilization in solutions of certain aromatic surfactants and polymers. Adsorption of dyes is often considered as a model system for organic pollutants removal using carbon nanotubes.

Usually, the adsorption capacity is large and strongly depends on pH meaning that protons concentration affects the structure of the CNT-dye complexes.[27] There is, however, a lack of detailed microscopic studies in the literature, at least concerning interaction of CR with CNTs, giving direct insights into that structure and its changes with pH.

Therefore, we performed extensive MD studies of CR-CNT conjugates for various pH conditions. Similarly like in the previous section we considered three cases pH3, pH4, pH5 differing in amounts of protonated and deprotonated forms of CR. We also considered 2 types of CNTs, namely: narrow nanotube with chirality (10,0) and wider nanotube with chirality (30,0). The diameters of these nanotubes were 7.8 Å and 23.5 Å, respectively, whereas their lengths were 82 Å. In both cases the nanotubes were described by the aiREBO potential[21] thus, depending on local forces, they could undergo deformations. Due to quite large dimensions of the nanotubes the chirality is a factor which mainly controls their diameters. Subtle effects coming from different atomic structure of tips and sidewalls, controlled by a given chirality parameters, are negligible compared to the effects of interaction of a big CR molecule with a large subset of carbon atoms belonging to the nanotube.

Figures 4-6 show simulations snapshots for various combinations of CNTs and pH conditions. They also inform about energetics of the obtained structures. Thus, $U_{CR\text{-}CR}$ is the mean interaction energy (potential) between two CR molecules, $U_{CR\text{-}CNT}$ is the mean interaction energy of CR molecule with carbon nanotube, whereas U_T is the mean potential energy of CR molecule coming from all interaction types in the system, these include the Lennard-Jones and electrostatic interactions between a given CR and other CR molecules, CNT, water, Na^+ and Cl^- ions. The results presented in Figs. 4-6 were verified by running the simulations twice. We have not observed significant differences in qualitative and quantitative results in both independent runs.

Analysis of Figs. 4-6 leads to a few interesting qualitative conclusions concerning the structure of the CR-CNT agglomerates. Namely, in the case of narrow nanotubes the CR molecules tend to preserve their micellar structures whereas in the case of wide nanotubes the micelles decompose and CR adsorbs on CNT surface individually forming a monolayer film. Such an arrangement enhances the interaction between aromatic carbons in CR molecule and carbon nanotube sidewall, thus this is an indication of the discussed π- π stacking which, according to the assumed classical force field, is purely dispersion interaction induced effect.

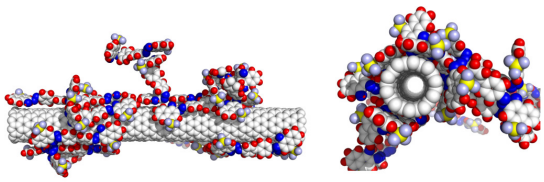

U_{CR-CR} = 315 kJ/mol, U_T=-558 kJ/mol, U_{CR-CNT}=-110 kJ/mol

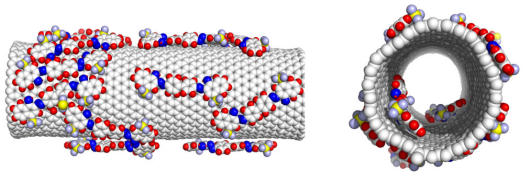

U_{CR-CR} = 307 kJ/mol, U_T=-574 kJ/mol, U_{CR-CNT}=-247 kJ/mol

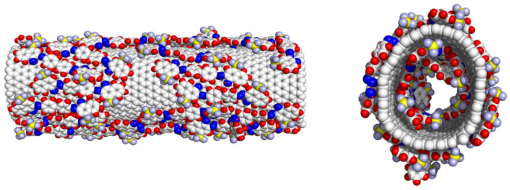

U_{CR-CR} = 480 kJ/mol, U_T=-575 kJ/mol, U_{CR-CNT}=-245 kJ/mol

Figure 4. Simulation snapshots for the system pH5 containing (from the top to the bottom): (10,0) CNT and 20 CR molecules, (30,0) CNT and 20 CR molecules, (30,0) CNT and 40 CR molecules. Simulation temperature was 310 K and ionic strength of solution was 0.145 mol $L^{-1.}$

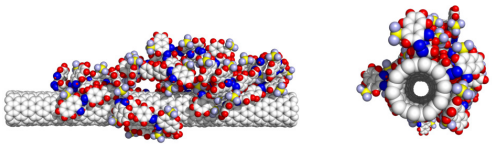

U_{CR-CR} =-267 kJ/mol, U_T=-895 kJ/mol, U_{CR-CNT}=-97 kJ/mol

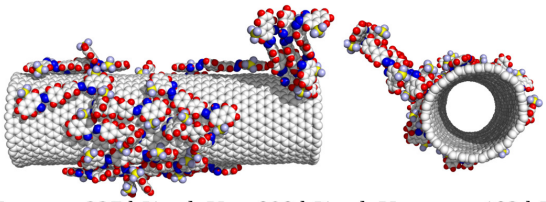

U_{CR-CR} =-227 kJ/mol, U_T=-898 kJ/mol, U_{CR-CNT}=-183 kJ/mol

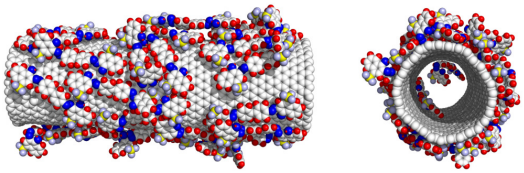

U_{CR-CR} =-228 kJ/mol, U_T=-900 kJ/mol, U_{CR-CNT}=-180 kJ/mol

Figure 5. Simulation snapshots for the system pH4 containing (from the top to the bottom): (10,0) CNT and 20 CR molecules, (30,0) CNT and 20 CR molecules, (30,0) CNT and 40 CR molecules. Simulation temperature was 310 K and ionic strength of solution was 0.145 mol L^{-1}.

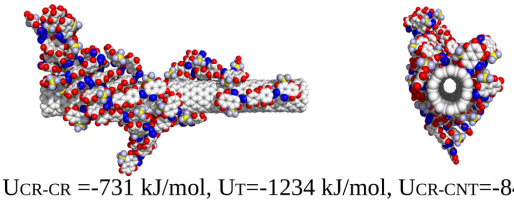

U_{CR-CR} =-731 kJ/mol, U_T=-1234 kJ/mol, U_{CR-CNT}=-84 kJ/mol

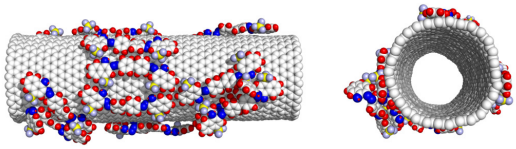

U_{CR-CR} =-541 kJ/mol, U_T=-1231 kJ/mol, U_{CR-CNT}=-218 kJ/mol

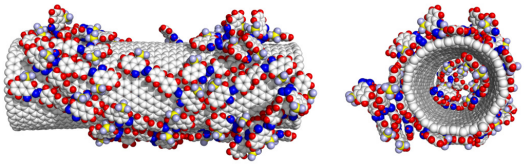

U_{CR-CR} =-645 kJ/mol, U_T=-1234 kJ/mol, U_{CR-CNT}=-192 kJ/mol

Figure 6. Simulation snapshots for the system pH3 containing (from the top to the bottom): (10,0) CNT and 20 CR molecules, (30,0) CNT and 20 CR molecules, (30,0) CNT and 40 CR molecules. Simulation temperature was 310 K and ionic strength of solution was 0.145 mol L^{-1}.

We can also notice that wider nanotubes with chirality (30,0) undergo strong deformations being the result of interaction with CR and with water molecules. The (10,0) CNTs are more rigid and their deformations are not so highly visible in static simulation snapshots. The inner space of (10,0) nanotubes is inaccessible to CR molecules, however, the (30,0) CNTs provide enough space for suction of guest molecules as seen in simulation snapshots. The probability of suction is obviously concentration dependent but it seems to be pH dependent either. Clearly, in the case pH5 quite a large portion of CR molecules occupy the inner space of CNT. In other cases, the number of CR molecules residing inside the CNT is definitely smaller. This is due to a weaker interaction between CR molecules at pH5 and, as seen in the snapshot, they easily spread out on the CNT surface. In the pH4 and pH3 cases those interactions are stronger and CR molecules tend to form denser 2D structures on CNT surfaces.

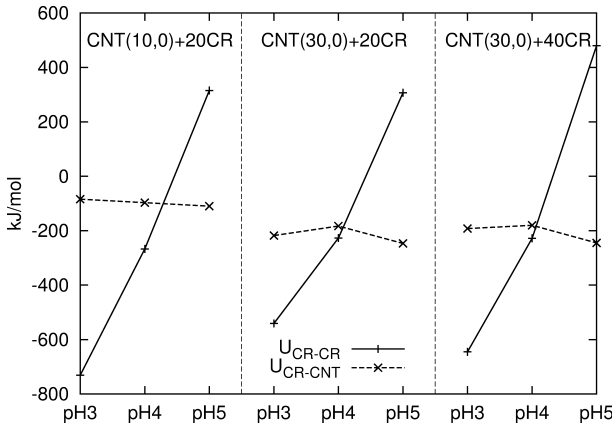

Figure 7. Mean energies of interactions between two CR molecules ($U_{CR\text{-}CR}$) and between CR molecule and CNT ($U_{CR\text{-}CNT}$) for various pH conditions. The error bars are normally smaller than the point sizes, so they are not plotted.

The relationships between pH conditions and interaction energies are shown in Fig. 7. Similarly like previously the deprotonated forms of CR reveal positive values of CR-CR interaction energy. Thus, they feel intermolecular repulsion, which, in turn is overcompensated by the interaction with the other components of the system (particularly with water molecules). Therefore, the total potential energy of a given CR molecule is negative (Figs. 2,4-6) and almost constant at given pH conditions. Lowering pH enhances attraction between CR molecules due to compensation of effective charges of individual molecules. The presence of CNT affects the CR-CR interaction due to the changes of the structure of CR ensemble. By comparing $U_{CR\text{-}CR}$ in Figs. 4-6 with U_{CC} in Fig.2 we can notice that (10,0) nanotube changes that energy only slightly so the CR cluster does not strongly alter its properties in the presence of such narrow nanotubes. Wider CNTs affect the CR-CR interaction energy strongly and we observe qualitative changes of CR structure in the presence of CNTs.

The strongest binding of CR to CNT is observed at conditions of higher pH, that is for the deprotonated forms of CR. Lowering pH reduces the $U_{CR\text{-}CNT}$ energy significantly in each case of pH. Moreover, for (30,0) nanotubes a maximum of $U_{CR\text{-}CNT}$ is observed for the pH4 case. It means that at conditions close to pKa, where CR exists in equal amounts of protonated and deprotonated forms, the biding is significantly weakened. The difference in binding energies between pH4 and pH5 is higher than 50 kJ mol^{-1} and it is accompanied by significant changes of CR surface structure. That effect might have important practical implications. Namely, due to tendency of formation of isolated islands on the surface upon lowering pH, the adsorption properties of CR film formed at higher pH will be strongly altered. It might lead to desorption (release) of some guest molecules entrapped in the CR network at higher pH. However, a more interesting behavior observed in the

case of wide nanotubes is the tendency to emptying the CNTs interiors at pH4 and pH3. The mechanism of that phenomena is quite clear, namely, at pH5 the CR molecules tend to spread out on the CNT walls because the CR-CR interaction is repulsive. Therefore, they easily penetrate the inner space of CNT due to enhanced attraction in the cylindrical space of the CNT. Lowering pH leads to switching CR-CR interaction from repulsive to attractive and creation of denser CR structures. It turns out that the tendency to creation of that densely packed external layer prevails over the enhanced attraction with the inner nanotube walls. As a result the CR molecules escape from the inner space of the CNT in favor of enhancing the contact with that external densely packed layer.

Potentially, that effect can be utilized in processes of pH triggered uncorking of nanotubes and subsequent release of guest molecules encapsulated in their inner cavities. Thus, the CR-CNT conjugates reveal potential properties of pH controlled drug delivery system. However, that conclusion needs further and dedicated calculations because the observed phenomenon seems to be highly dependent on CNT geometry and CR concentration. Also, the presence of other guest molecules in the CNT may destroy that subtle energetic balance responsible for the observed phenomenon.

It would also be useful to check whether transition from the corked state at pH5 into uncorked one at pH3 (using as input the structure obtained at pH5) occurs in times available to probe in MD simulations. Unfortunately, changing pH requires substantial changes of CR molecule topology, charge distribution, the number of counterions, etc. Thus, in the present construction of the simulation box such a transition is not feasible to do. So, we need to rely on the results corresponding to thermodynamic equilibrium.

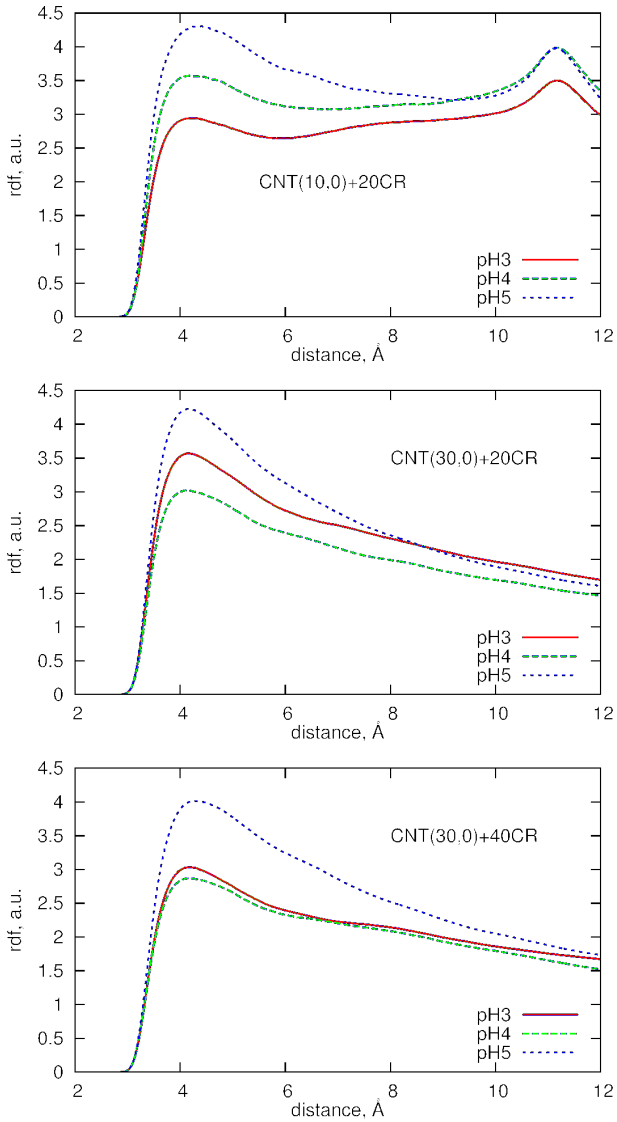

Figure 8. Radial distribution functions (rdf) between aromatic carbons of CR and CNT for the studied systems.

Analysis of radial distribution functions between CR and CNT (Fig.8) gives another portion of useful information about the structure of CR-CNT conjugates. Namely, we can see that the density of CR adsorbed on the CNTs differs qualitatively for (10,0) and (30,0) nanotubes. In the former case there are two peaks; the first one corresponds to adsorption of CR on the CNT surface, however, the second one informs that CR creates dense structures at long distances from the CNT as well. As seen in simulation snapshots those dense structures are due to formation of fragments of CR micelles in the bulk and not interacting directly with CNT. Lowering pH gradually reduces the density in the vicinity of the CNT meaning that at low pH binding of CR micelles to CNTs is weakened in favor of developing bulky clusters of CR.

Wider nanotubes lead to qualitatively different results. However, we still see the highest density of CR in the case pH5, thus, biding of CR to CNT is the strongest in this case. Lowering pH

in those cases gives similar effect like in Fig. 7. Namely, the smallest adsorption of CR occurs for the pH4 case and it slightly increases for still lower pH conditions, that is for the pH3 case. That effect is particularly visible for the relatively low concentration of CR (20 CR molecules), higher concentration (40 CR molecules) leads to very similar density profiles for pH4 and pH3 cases. However, a general conclusion coming from Fig. 8 is that adsorption of CR on CNT surfaces is weakened at lower pH conditions and that effect is consistent with the energy profiles shown in Fig. 7.

3.4 Thermodynamics of CR adsorption on CNTs

Analysis of potential energy changes, as discussed in previous section, does not provide a definite answer concerning the thermodynamic stability of the considered systems. This is due to usual limitation of computational methods as they probe only limited timescales or phase space sections. The decisive parameters which inform about thermodynamic stability of a system under investigation are free energy or enthalpy changes related to a given system state. Therefore, in this section we discuss how these important physical parameters are affected by pH conditions, CNT type or density of CR adsorbed on CNTs.

Among many methods of determination of free energy from molecular simulations the thermodynamic integration[28] is the most appropriate in this case. This is because we are interested in a global free energy change accompanied to desorption of CR from CNTs. That transition (reaction path) can be adequately represented by the so-called alchemical transformation, i.e. some part of system hamiltonian is rescaled in such a way that we obtain a transition of the initial state (unscaled hamiltonian) to the final state through a series of intermediate (unphysical) states. In the particular case of the decomposition of CR-CNT conjugates we introduce the scaling factor to the part of the hamiltonian which is responsible for CNT interactions with CR and other components of the system. Thus, the scaled hamiltonian reads,

$$H_s = H_{ns} + f(\lambda)H_{CNT} \quad (1)$$

H_{CNT} is actually the Lennard-Jones potential acting between carbons belonging to CNT and other components of the system. This is because the CNTs are composed of neutral carbon atoms and thus electrostatic interaction part does not exist in that case. H_{ns} contains all other interaction types existing in the system and not affected by the scaling protocol. The function $f(\lambda)$ has the usual meaning of the scaling factor being a function of the reaction coordinate λ and we assumed the following expression for its analytical form:[28]

$$f(\lambda) = (1 + \lambda(\eta - 1))^2 \quad (2)$$

Thus, when making the alchemical transformation by increasing λ from 0 to 1 the system runs from fully interacting initial state to a very weakly interacting final state at λ = 1. For the assumed value η = 0.1 the nanotubes actually disappear because their interaction with the rest of the system is reduced by two orders of magnitude in the depths of the Lennard-Jones potential. The free energy difference between these two states can be determined according to the thermodynamic integration concept, that is

$$\Delta A = \int \left\langle \frac{dH_s}{d\lambda} \right\rangle_\lambda d\lambda \qquad (3)$$

Thus, in order to calculate ΔA it is necessary to perform numerical integration of the derivative of the scaled hamiltonian with respect to λ. The integrand in (3) can be determined from simulation as a mean value of

$$\left\langle \frac{H_s - H_{ns}}{f(\lambda)} \frac{df(\lambda)}{d\lambda} \right\rangle_\lambda \qquad (4)$$

thus, every point in numerical integration needs a separate simulation run.

In order to determine the free energy change associated with the desorption of CR from CNT we assumed the following thermodynamic cycle. First, the CNT is transfered into vacuum, according to the alchemical transformation methodology, by weakening all its interactions with the environment. Internal degrees of freedom of the CNT were not affected so after the thermodynamic integration we got the free energy change associated with the removal of the CNT from the system, ΔA_1. In the second stage of the cycle we gradually enhanced the interaction of CNT with the solvent, so at λ = 1 we got fully solvated but isolated CNT and CR. Thus, after thermodynamic integration we got ΔA_2 which corresponds to free energy change associated with the transfer of the CNT to the solvent. Next, by taking the difference $\Delta A = \Delta A_1 - \Delta A_2$ we obtain the free energy change associated with the desorption of CR from the CNT in the considered solvent. Fig. 9 shows the values of ΔA determined for all systems considered in this work.

As mentioned the ΔA values give a notion about total free energy changes associated with the detachment of all CR molecules from the CNT. It is, however, also interesting to learn what is the mechanism of a single molecule desorption, particularly, how the free energy of detachment changes with the distance from the CNT walls. In order to study that mechanism we employed the umbrella sampling and the weighted histogram analysis methods.[29]

The starting point in this part of calculations was selection of the CR molecule to which the umbrella potential is added. We took the molecule which was adsorbed possibly far away from the CNT tips and oriented along the CNT axis. The biasing potential (harmonic) was imposed on the molecule center of mass and it acted in the direction perpendicular to the CNT axis. By controlling

the position of the biasing potential minimum we could shift the selected molecule to a prescribed distance from the CNT and next we could collect the probability distribution of that biased configuration. By collecting the probability distributions in a number of sampling windows for various distances of the CR molecule from the CNT axis we could determine the potential of mean force (pmf) by performing weighted histogram analysis in all sampling windows.[29] Due to enormous computational work required for determination of the full pmf we focused only on two systems: (30,0) CNT and containing 20 fully protonated CR molecules and (30,0) CNT with 40 fully deprotonated CR molecules. Results of those calculations are shown in Fig.9.

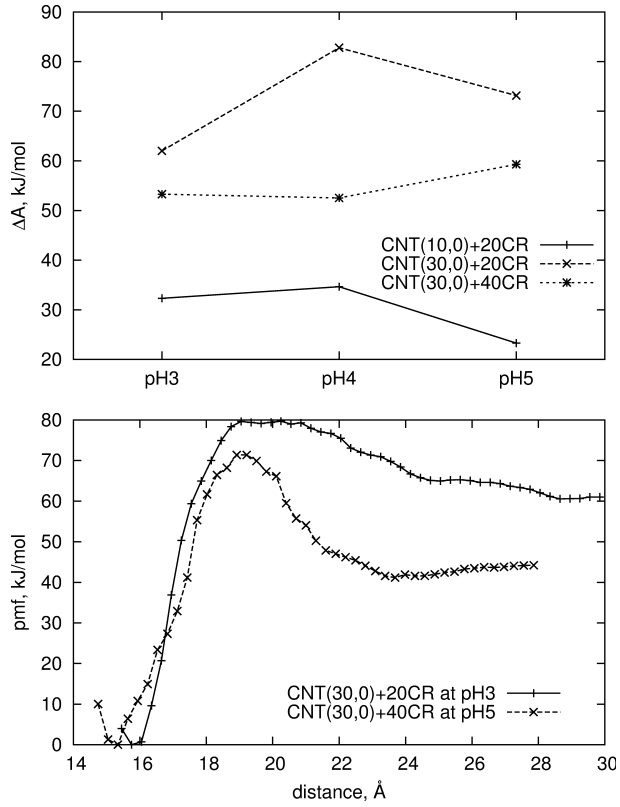

Figure 9. Free energy changes associated with the desorption of CR from the CNT determined using thermodynamic integration (top) and potential of mean force associated with the detachment of a single CR molecule from the CNT surface determined using umbrella sampling and weighted histogram analysis methods (bottom).

Results shown in Fig.9 demonstrate that in all cases adsorption of CR on the CNT surfaces is stable at the considered conditions. The range of free energy changes strongly depends on the CNT parameters. Adsorption on the narrow nanotube (10,0) is definitely weaker than on the wider one and it is very likely that at elevated temperatures the CR-CNT complex can undergo spontaneous decomposition. In the case of (30,0) nanotubes the CR-CNT conjugates turn out to be very stable though the number of the adsorbed dye molecules affects the free energy significantly.

The ΔA values in Fig.9 are recalculated per single CR molecule, thus, we can see that higher concentrations of CR destabilize the system when comparing to the case of lower number of adsorbed molecules. However, the free energy change associated with the desorption of CR is very high in both cases and thermodynamically such a process is strongly unfavored. Very interesting are free energy changes for the same system but at various pH conditions. In any case we observe either maximum or minimum for pH4. Because the free energy carries a complex information depending on many factors it is difficult to extract a decisive one and responsible for existing of those extreme values of ΔA. The existence of maximum in ΔA can be (probably) attributed to the opposite action of protonation of CR in modification of the interactions between CR molecules and with the solvent. High pH means hydrophilic state of CR and transfer to the desorbed hydrophilic clusters of CR costs less than transfer from partially neutralized conjugate at pH4 case. Similarly, at very low pH when CR become more hydrophobic and tends to form big ribbon-like micelles the cost of creation of such charge-neutral micelles is smaller than partially charged micelles at pH4. Thus, the case pH4 is a kind of compromise between these two limiting cases and therefore the system reveals the highest free energy of decomposition.

The case of high concentration of CR (40 molecules) reveals different trend in free energy changes with pH. In this case another effect seems to be decisive. At high pH the CR molecules form a monomolecular layer inside and outside the CNT. Thus, the hydrophobic surface of CNT becomes screened and the whole system becomes hydrophilic. That is why the case pH5 turns out to be the most stable. Lowering pH leads to formation of islands of CR clusters on the CNT surface, thus making some part of CNT surface uncovered. Therefore the systems pH4 and pH3 become less stable than pH5 and they reveal very similar ΔA values.

Analysis of pmf curves gives another portion of useful information. Namely, in both analyzed cases we observe distinct activation barriers for detachment of the CR molecule from the CNT surface. The differences between pmf values at adsorbed state and at full separation, which are equivalent to free energy changes associated with the detachment, are comparable to ΔA values determined from thermodynamic integration. In the case of the system pH3 both values are almost identical. Formally, they should be the same because the free energy change cannot depend on the choice of the determination method. However, we should take into account that both methods probe quite different reaction pathways and therefore they can produce different results. In the case of thermodynamic integration we probe an average free energy change during the process of detachment of all CR molecules from the CNT whereas the umbrella sampling method probes detachment of a single particle. Thus, comparable values of free energy change for the case pH3 mean that, on average, all adsorbed molecules reveal similar energetic state. This is understandable

since all molecules are located on the external surface of the CNT (see Fig.6). In the case pH5 there are many molecules adsorbed inside the CNT and, obviously, their energetic state is different that those on the external surface. Thus, the average ΔA is different than the pmf change determined for the molecule detached from the external surface.

Smaller value of free energy change, determined for a single molecule, than the average value implies that desorption from the inner cavity of the CNT needs more energy. This is fully understandable and consistent conclusion. Less obvious is a high activation barrier for desorption found in the case pH5. Because interaction between adsorbed CR molecules has strong repulsive component, $U_{CR\text{-}CR}$ (Figs. 4 and 7) it is expected that desorption proceeds without or with only minor activation barrier. However, as seen in Fig. 9, the barrier for desorption is only about 10 kJ mol^{-1} less than that in the case pH3 and reaches 70 kJ mol^{-1}. The activation barriers for desorption of the order 70 - 80 kJ mol^{-1} mean that spontaneous desorption is highly unlikely at the considered conditions. Moreover, also adsorption process is accompanied by significant activation barriers. They are about 20 kJ mol^{-1} for the pH3 case and about 25 kJ mol^{-1} for pH5. Those barriers are related to the need of creation of free place on the CNT for adsorption of the molecule. In the case of pH5 the barrier is slightly larger, most probably due to the higher density of CR molecules on the surface.

4. Summary

Congo red interacts strongly with carbon nanotubes. The range of that interaction depends on several factors. The most prominent is the nanotube diameter which affect the adsorption mechanism either qualitatively or quantitatively. Narrow nanotubes with chirality (10,0) are impenetrable to CR molecules due to steric factors. In that case the interaction energy and stability of adsorption is the smallest, though, strong enough to keep the CNT-CR conjugates stable at the considered conditions. Lowering pH, or making the CR more and more protonated, affect the structure of the adsorbed CR, however, that effect is more pronounced in case of wider nanotubes. Those wider CNTs provide enough space for encapsulation of CR inside their inner cavities. Additionally, due to smaller curvature of the sidewalls adsorption of CR is much stronger than on the narrow (10,0) nanotubes. Wider (30,0) nanotubes represent particularly interesting case; it was found that CR molecules tend to spread out on their surfaces thus the ribbon-like clusters of free CR decompose no matter what are pH conditions. The CR-CNT conjugates reveal very high values of free energy change associated with the desorption, thus the conjugates are highly stable from the thermodynamic point of view. Moreover, we found very high activation barriers for detachment of a CR molecule; the barriers exist for the adsorption process as well but their values are not big, i.e. 20

-25 kJ mol^{-1}. Particularly interesting and potentially useful conclusion comes from analysis of the structure of the adsorbed CR as a function of pH. We found that at higher pH, corresponding to fully deprotonated form of CR, filling of inner cavities of CNTs occurs spontaneously. However, lowering pH by setting some number of CR molecules protonated leads to spontaneous escape of CR molecules from the CNT interior. This phenomenon is reversible and does not need any biasing potential to occur. Thus, it might be used for pH controlled locking/unlocking of some other molecules encapsulated inside CNTs. This hypothesis will be carefully analyzed in our ongoing research.

5. Acknowledgments

This work was supported by Polish National Science Centre grant UMO-2012/07/E/ST4/00763. A. J. acknowledges the financial support from the project Interdisciplinary PhD Studies "Molecular sciences for medicine" (co-financed by the European Social Fund within the Human Capital Operational Programme).

6. References

[1] J.L. Hudson, M.J. Casavant, J.M. Tour, Water-Soluble, Exfoliated, Nonroping Single-Wall Carbon Nanotubes*, J. Am. Chem. Soc.* 2004, **126**, 11158–11159.

[2] C.A. Dyke, J.M. Tour, Unbundled and Highly Functionalized Carbon Nanotubes from Aqueous Reactions, *Nano Lett.* 2003, **3**, 1215–1218.

[3] R.J. Chen, Y. Zhang, D. Wang, H. Dai, Noncovalent Sidewall Functionalization of Single-Walled Carbon Nanotubes for Protein Immobilization, *J. Am. Chem. Soc.* 2001, **123**, 3838–3839.

[4] C. Hu, Z. Chen, A. Shen, X. Shen, J. Li, S. Hu, Water-soluble single-walled carbon nanotubes via noncovalent functionalization by a rigid, planar and conjugated diazo dye, *Carbon* 2006, **44**, 428–434.

[5] Z. Song, J. Dai, S. Zhao, Y. Zhou, F. Su, J. Cui, et al., Aqueous dispersion of pristine single-walled carbon nanotubes prepared by using a vinylimidazole-based polymer dispersant, *RSC Adv.* 2014, **4**, 2327.

[6] P. Liu, Modification Strategies for Carbon Nanotubes as a Drug Delivery System, *Ind. Eng. Chem. Res.* 2013, **52**, 13517–13527.

[7] C.L. Lay, J. Liu, Y. Liu, Functionalized carbon nanotubes for anticancer drug delivery, *Expert Rev. Med. Devices* 2011, **8**, 561–566.

[8] P. Spólnik, B. Stopa, B. Piekarska, A. Jagusiak, L. Konieczny, J. Rybarska, et al., The Use of

Rigid, Fibrillar Congo Red Nanostructures for Scaffolding Protein Assemblies and Inducing the Formation of Amyloid-like Arrangement of Molecules: Use of Rigid, Fibrillar Congo Red Nanostructures, *Chem. Biol. Drug Des.* 2007, **70**, 491–501.

[9] B. Stopa, A. Jagusiak, L. Konieczny, B. Piekarska, J. Rybarska, G. Zemanek, et al., The use of supramolecular structures as protein ligands, *J. Mol. Model.* 2013, **19**, 4731–4740.

[10] G. Pastorin, W. Wu, S. Wieckowski, J.-P. Briand, K. Kostarelos, M. Prato, et al., Double functionalisation of carbon nanotubes for multimodal drug delivery, *Chem. Commun.* 2006, 1182.

[11] T. Panczyk, T. Da Ros, G. Pastorin, A. Jagusiak, J. Narkiewicz-Michalek, Role of Intermolecular Interactions in Assemblies of Nanocontainers Composed of Carbon Nanotubes and Magnetic Nanoparticles: A Molecular Dynamics Study, *J. Phys. Chem. C* 2014, **118**, 1353–1363.

[12] V.V. Chaban, O.V. Prezhdo, Water Boiling Inside Carbon Nanotubes: Toward Efficient Drug Release, *ACS Nano* 2011, **5**, 5647–5655.

[13] M. Król, T. Borowski, I. Roterman, B. Piekarska, B. Stopa, J. Rybarska, et al., Force-field parametrization and molecular dynamics simulations of Congo red, *J. Comput. Aided Mol. Des.* 2004, **18**, 41–53.

[14] A.D. MacKerell,, D. Bashford, Bellott, R.L. Dunbrack,, J.D. Evanseck, M.J. Field, et al., All-Atom Empirical Potential for Molecular Modeling and Dynamics Studies of Proteins, *J. Phys. Chem. B* 1998, **102**, 3586–3616.

[15] Y. Duan, C. Wu, S. Chowdhury, M.C. Lee, G. Xiong, W. Zhang, et al., A point-charge force field for molecular mechanics simulations of proteins based on condensed-phase quantum mechanical calculations, *J. Comput. Chem.* 2003, **24**, 1999–2012.

[16] J. Wang, R.M. Wolf, J.W. Caldwell, P.A. Kollman, D.A. Case, Development and testing of a general amber force field, *J. Comput. Chem.* 2004, **25**, 1157–1174.

[17] J. Wang, W. Wang, P.A. Kollman, D.A. Case, Automatic atom type and bond type perception in molecular mechanical calculations, *J. Mol. Graph. Model.* 2006, **25**, 247–260.

[18] C.I. Bayly, P. Cieplak, W. Cornell, P.A. Kollman, A well-behaved electrostatic potential based method using charge restraints for deriving atomic charges: the RESP model, *J. Phys. Chem.* 1993, **97**, 10269–10280.

[19] C. Wu, Z. Wang, H. Lei, W. Zhang, Y. Duan, Dual Binding Modes of Congo Red to Amyloid Protofibril Surface Observed in Molecular Dynamics Simulations, *J. Am. Chem. Soc.* 2007, **129**, 1225–1232.

[20] Water model - Wikipedia, the free encyclopedia, http://en.wikipedia.org/wiki/Water_model

(accessed January 8, 2014).

[21] S.J. Stuart, A.B. Tutein, J.A. Harrison, A reactive potential for hydrocarbons with intermolecular interactions, *J. Chem. Phys.* 2000, **112**, 6472.

[22] S. Plimpton, Fast Parallel Algorithms for Short-Range Molecular Dynamics, *J. Comput. Phys.* 1995, **117**, 1–19.

[23] C.E. Bonancêa, G.M. do Nascimento, M.L. de Souza, M.L.A. Temperini, P. Corio, Substrate development for surface-enhanced Raman study of photocatalytic degradation processes: Congo red over silver modified titanium dioxide films, *Appl. Catal. B Environ.* 2006, **69**, 34–42.

[24] M. Skowronek, B. Stopa, L. Konieczny, J. Rybarska, B. Piekarska, E. Szneler, et al., Self-assembly of Congo Red—A theoretical and experimental approach to identify its supramolecular organization in water and salt solutions, *Biopolymers* 1998, **46**, 267–281.

[25] S. Woodcock, B. Henrissat, J. Sugiyama, Docking of congo red to the surface of crystalline cellulose using molecular mechanics, *Biopolymers* 1995, **36**, 201–210.

[26] A. Star, T.-R. Han, J.-C.P. Gabriel, K. Bradley, G. Grüner, Interaction of Aromatic Compounds with Carbon Nanotubes: Correlation to the Hammett Parameter of the Substituent and Measured Carbon Nanotube FET Response, *Nano Lett.* 2003, **3**, 1421–1423.

[27] Y. Yao, H. Bing, X. Feifei, C. Xiaofeng, Equilibrium and kinetic studies of methyl orange adsorption on multiwalled carbon nanotubes, *Chem. Eng. J.* 2011, **170**, 82–89.

[28] D.M. Eike, E.J. Maginn, Atomistic simulation of solid-liquid coexistence for molecular systems: Application to triazole and benzene, *J. Chem. Phys.* 2006, **124**, 164503.

[29] S. Kumar, J.M. Rosenberg, D. Bouzida, R.H. Swendsen, P.A. Kollman, THE weighted histogram analysis method for free-energy calculations on biomolecules. I. The method, *J. Comput. Chem.* 1992, **13**, 1011–1021.